Potassium fluoride postdeposition treatment with etching step on both Cu-rich and Cu-poor $CuInSe_2$ thin film solar cells

Finn Babbe,* Hossam Elanzeery, Michele Melchiorre, Anastasiya Zelenina, and Susanne Siebentritt
Laboratory for Photovoltaics, Physics and Materials Science Research Unit, University of Luxembourg, Belvaux, L-4422, Luxembourg

(Received 21 February 2018; revised manuscript received 1 June 2018; published 24 October 2018)

Recent progress in the power conversion efficiency of $Cu(In, Ga)Se_2$ thin film solar cells has been achieved by an alkali postdeposition treatment. This treatment has been shown to change the surface composition and structure as well as the bulk properties. To investigate the relative importance of those two effects we study the impact of the treatment on Cu-rich and Cu-poor $CuInSe_2$, which show a different influence of interface recombination without the treatment. We develop a potassium postdeposition treatment that can be applied to Cu-rich material, where an additional etching step is necessary. The same postdeposition treatment with etching step is applied to Cu-poor material. In both cases we observe an increase of the power conversion efficiency and open circuit voltage. Comparing the increase in open circuit voltage to the increase in quasi-Fermi level splitting indicates that the improvement in Cu-poor solar cells is mostly due to changes in the bulk, whereas in Cu-rich solar cells both the bulk and the interface are improved. The improvement of the interface is corroborated by temperature dependent current-voltage characteristics, which show that the dominating recombination path in Cu-rich solar cells moves from the interface to the bulk after treatment and by admittance spectroscopy, which shows that the treatment removes a 200 meV deep defect. Photoluminescence spectroscopy shows that even in Cu-rich material the alkali treatment creates a Cu-poor surface, which in this case cannot be created by diffusion of Cu into the bulk, but is grown during the treatment.

DOI: 10.1103/PhysRevMaterials.2.105405

I. INTRODUCTION

Copper indium gallium di-selenide, $Cu(In, Ga)Se_2$ or CIGS, represents the most efficient absorber for thin film solar cells, reaching power conversion efficiencies (PCE) up to 22.9% on the laboratory scale [1,2]. The latest improvements in PCE have been achieved by employing an alkali fluoride postdeposition treatment (PDT), especially potassium fluoride (KF) [3]. The ternary compound copper indium di-selenide (CIS) is less complex compared to CIGS, making it a good material to study the manifold effects of a KF PDT. CIS has a lower bandgap and shows PCE up to 15% [4]. $CuInSe_2$ and $Cu(In, Ga)Se_2$ can be grown under Cu-poor or Cu-rich conditions that result in very different semiconductor properties. Solar cells are generally made of Cu-poor material, since it results in better PCEs [5]. In the past we have demonstrated, however, that the semiconductor properties of absorbers grown under Cu-excess are favorable compared to Cu-poor ones [5]: less compensation, lower defect densities, no electrostatic potential fluctuations, higher mobilities, and larger grains. Nevertheless, it has long been known that the absorbers grown under Cu-excess exhibit problematic surface properties, which lead to recombination at or near the interface [6]. Recently we demonstrated by investigating the quasi-Fermi level splitting that not only the surface is problematic in Cu-rich absorbers [7], but also the bulk shows higher recombination rates. Still, Cu-rich solar cells show a much higher difference between quasi-Fermi level splitting and open circuit voltage V_{OC} than Cu-poor ones, indicating that the interface of Cu-rich cells remains a problem. To improve the interface we have employed an indium selenide (In-Se) surface treatment which leads to a CIS solar cell with a "Cu-rich" bulk and a Cu-poor surface [8–10] that has the same efficiency compared to our Cu-poor solar cells. Now, it was shown that the KF postdeposition treatment also leads to a Cu-depleted surface, at least in Cu-poor absorbers [3]. However, the KF treatment as it is generally used, cannot be directly transferred to Cu-rich absorbers, because these require an etching step. From the phase diagram of $CuInSe_2$ [11], it can be seen that the compound can be formed in a broad compositional range in the Cu-poor region ([Cu]/[In] < 1), whereas absorbers grown under Cu-excess form a stoichiometric bulk of CIS together with a secondary copper selenide (Cu_xSe) phase at the surface. This secondary phase is highly conductive and has to be etched using potassium cyanide (KCN) [12,13] before solar cell processing. It was shown that cyanide etching removes Cu selenides, even from the grain boundaries [12]. KCN etched absorbers grown under Cu-excess will be referred in the text as "Cu-rich" for easy differentiation. To perform a KF postdeposition treatment, the films have to be removed from the growth chamber and etched. Therefore our first attempt was a KF postdeposition treatment, where we deposit KF and then transfer the film to an annealing oven, where the surface

*Author to whom correspondence should be addressed: Finn.Babbe@uni.lu

was annealed with additional Se [14]. This *ex situ* KF PDT also lowers the copper content at the surface of the absorber, independent of whether the absorber was Cu-poor or "Cu-rich" and improves the absorber/CdS heterojunction quality. The *ex situ* treatment leads to an increase in V_{OC} for both "Cu-rich" and Cu-poor CIS samples. The hygroscopic nature of KF and the necessary transport through air after the KF deposition and before the subsequent annealing, however, lead to a higher series resistance, reduced fill factor (FF) and a higher diode factor, preventing an efficiency gain, as was observed by other groups as well [15]. To overcome the problems of the *ex situ* treatment and still be able to benefit from the treatment, a third and new process route is introduced in this contribution. It is labeled "potassium fluoride postdeposition treatment with etching step" and consists of the following steps: First, after the absorber is processed, it is fully cooled down and removed from the vacuum chamber. Second, in a cyanide etching step the secondary phases are removed from the absorber surface. Third, the etched samples are immediately introduced back to the growth chamber. Finally, the etched samples are heated up under selenium atmosphere to roughly 390 °C. At this temperature, KF is deposited and the samples are annealed inside the growth chamber. We demonstrate here that this treatment in fact leads to an improvement of the efficiency, not only the V_{OC} of "Cu-rich" solar cells, but also for Cu-poor ones. The bulk and the interface of the "Cu-rich" absorbers are improved. Furthermore, we will conclude from the experiments that the Cu-poor surface grows on top of the original surface, and is not formed by diffusion of Cu into the bulk away from the surface.

II. MATERIAL AND METHODS

A. Preparation of $CuInSe_2$ solar cells

Polycrystalline CIS absorbers are grown on molybdenum coated soda lime glass through a one-stage coevaporation process at a substrate temperature of 530 °C in a molecular beam epitaxy (MBE) system. The copper flux is controlled to obtain a Cu/In ratio between 0.85 and 0.92 for Cu-poor samples and between 1.2 and 1.3 for "Cu-rich" samples [16]. The elemental composition is determined by energy dispersive x-ray spectroscopy (EDX) at 20 keV excitation and represents the average composition of the absorber including Cu_xSe, if present. After growth, the "Cu-rich" samples are etched using a 10% aqueous solution of KCN for 5 min to remove the Cu_xSe phase (see supplementary material I [17] for SEM images and EDX data before and after etching), whereas the Cu-poor samples are etched for 30 sec in a 5% aqueous solution of KCN to remove residual oxides [12,18,19]. Furthermore, the Cu_xSe phase is observed in XRD on unetched samples and disappears completely from the XRD pattern in etched samples [20]. During the KF PDT, the samples are heated under selenium flux similar to the one used during absorber growth. At roughly 390°C substrate temperature, potassium fluoride is deposited with a rate of roughly 1 nm per min for several min. After treatment, the samples are rinsed with deionized water to remove residual fluorides and a thin CdS layer is deposited by chemical bath deposition (CBD). The duration of the CdS bath is variable and defined by turbidity change. The cell is finished by sputtering a layer of undoped zinc oxide and a second nominally undoped ZnO layer which is deposited under an additional plasma near the substrate [21]. This biased ZnO has a larger charge mobility while having the same resistivity compared to standard aluminium doped ZnO, leading to a higher transparency in the infrared region [22]. For better charge carrier extraction nickel aluminium contacting grids are evaporated on top of the window layer. In this contribution, we study the effects of three different durations of the KF PDT (4, 8, and 12 mins) on a "Cu-rich" grown absorber. For comparison and to confirm the validity, also the results of a 6-min treatment of a Cu-poor sample are presented. For determination of the quasi-Fermi level splitting (qFLs) a second set of absorbers with similar treatment conditions, which were covered with CdS after the PDT, were used.

B. Characterization methods

The current-voltage (IV) characteristics of finished solar cells are measured with a solar simulator using a silicon reference solar cell to adjust the incoming flux. The external quantum efficiency (EQE) is measured at room temperature using chopped illumination from a halogen/xenon lamp in front of a grating monochromator and a chopper. The photocurrent is measured with a lock-in-amplifier. For the extraction of the activation energy of the dominant recombination channel, a closed cycle helium cryostat was used to measure the IV spectra in a temperature range between 50 and 320 K, as measured on a dummy cell next to the device. The illumination intensity from a cold mirror halogen lamp was calibrated to match at room temperature the short circuit current density (J_{SC}) determined from IV under standard test conditions. The same setup was used to perform capacitance-voltage (CV) measurements as well as temperature dependent admittance (ADM). For the extraction of the qFLs, photoluminescence (PL) spectra are measured by a calibrated setup at room temperature under continuous monochromatic illumination of 660 nm wavelength. The emitted PL is collected by two off-axis mirrors, focused into an optical fiber, spectrally resolved in a grating monochromator and detected by an InGaAs-detector array. The calibration procedure for single photon counting and qFLs extraction can be found elsewhere [7,23,24]. A liquid helium flow cryostat is used to measure the photoluminescence at 10 K within the same PL setup. Scanning electron microscope (SEM) images are taken after KCN etching as well as after the postdeposition treatment, with a voltage of 7 kV. Cross-section electron microscope images were used to determine the thickness of the CdS layer.

III. RESULTS AND DISCUSSION

A. KF PDT with etching step on "Cu-rich" absorber layers

IV measurements have been carried out on "Cu-rich" absorbers with and without treatment with different durations. While the substrate temperature during treatment was kept constant, the duration of KF deposition was varied between 4 and 20 min. "Cu-rich" absorbers with KF treatments of more than 12 min show reduced efficiency mainly in terms of V_{OC} and FF compared to untreated ones. In order to optimize the KF PDT for "Cu-rich" absorbers, the characteristics of

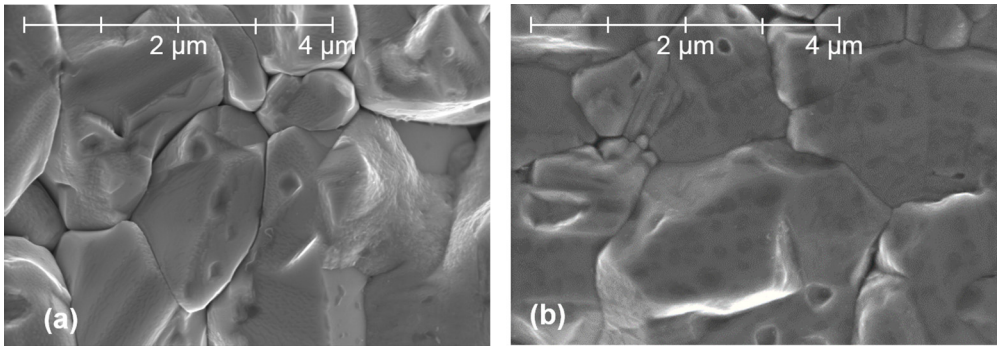

FIG. 1. Scanning electron microscope images of a "Cu-rich" grown absorber after etching (a) and the same absorber after an 8-min-long KF PDT (b).

three different KF treatment durations of 4, 8, and 12 min are studied in detail. Top view SEM pictures of the absorber before and after KF PDT show a change in surface morphology. The SEM images of an etched "Cu-rich" absorber and of the same absorber after an 8-min-long KF PDT are depicted in Fig. 1. A surface patterning on top of the grains is visible after treatment, similar to what has been observed on treated Cu-poor CIGS samples [25,26]. The patterning is the strongest for the sample with an 8-min-long treatment, but is also visible for 4- and 12-min-long treatments (see supplementary material II [17] for additional SEM images). This patterning indicates a similar effect of the treatment on the surface of "Cu-rich" and Cu-poor samples. The underlying crystal structure remains unchanged after KF PDT in both cases, determined from cross-section SEM images of finished devices (see supplementary material III [17] for cross-section SEM images).

Exemplary IV curves of the finished solar cells are plotted in Fig. 2 and the average electrical parameters of six cells for each of the untreated and treated absorbers deposited using the same substrate and the same fabrication conditions are presented in Table I. The IV parameters of the best solar cell are indicated in brackets.

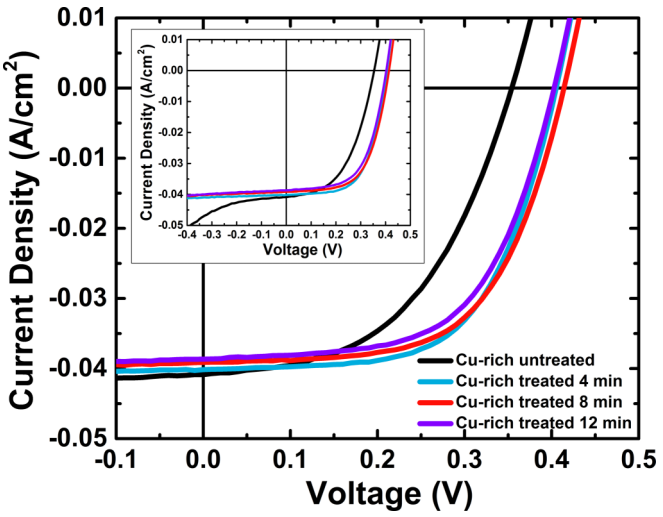

FIG. 2. IV characteristics of an untreated "Cu-rich" CIS solar cell and three KF treated cells where the alkali deposition lasted for 4, 8, and 12 min. The inset of the figure represents a wider voltage axis in the reverse range.

The PDT has several effects on the IV curves. Untreated "Cu-rich" cells show a reverse breakdown behavior with a strong increase of the reverse current that starts at reverse voltages as low as -0.2 V as observed in the inset of Fig. 2. This behavior was observed earlier and can be explained by a space-charge-limited current originating from the interface between the CIS and CdS layers [27]. This breakdown is not observed within the measured voltage range for any of the treated cells. The most prominent advantage of the KF PDT is the increase of the V_{OC} by 50 – 60 mV. This improvement is more pronounced than in the *ex situ* treatment of "Cu-rich" grown absorbers ($\Delta V_{OC} = 36$ mV) [14]. Moreover, the FF improves by 8–10 % absolute. This gain in FF is mainly due to a lower diode ideality factor (decreased from 1.9 to 1.6) and a strong increase in the shunt resistance (from 120 Ω/cm^2 to values between 900 Ω/cm^2 and 1400 Ω/cm^2), extracted by fitting the dark IV curve with the single diode model of the Energy Research Centre of the Netherlands (ECN) IV curve fitting program IVFIT [28]. Unlike the *ex situ* treatment where the series resistance (R_S) increased significantly after the treatment [14], the KF PDT with etching step increases the series resistance only slightly. The short circuit current density (J_{SC}) is increased for the shortest treatment duration and decreased for the two longer durations. The decrease can be explained by the EQE spectra shown in Fig. 3(a).

The same drop of the quantum efficiency in the short wavelength region is observed for all treated samples. In literature, a faster CdS growth on CIGS samples with KF PDT has been reported, which leads to a thicker CdS layer and more parasitic absorption [29]. To validate this also for the ternary CIS, cross-section SEM images of finished devices are taken. For the untreated sample, a thickness of the CdS layer of (35 ± 2) nm is determined, whereas the treated samples exhibit a (48 ± 3)-nm-thick CdS layer. The faster CdS growth on absorbers layers with KF PDT can thus be confirmed also for stoichiometric CIS. While the increase in the buffer layer thickness is responsible for the decrease in the EQE response on all treated samples for the short wavelength region, the behavior of the treated samples in the longer wavelength region can be attributed to optical and carrier recombination losses [30]. For all treated samples, a 200 meV defect has been removed as indicated below by the admittance measurements. This defect acts as a recombination center [31] as presented in

TABLE I. IV parameters under standard test conditions for the average of six solar cells for each of the untreated and KF treated "Cu-rich" CIS where the alkali deposition lasted 4, 8, and 12 min. Values in brackets represent the IV parameters of the best solar cell.

Sample	Efficiency (%)	FF (%)	V_{OC} (mV)	J_{SC}(mA/cm^2)	R_S(Ω/cm^2)	R_{Sh}(Ω/cm^2)
No PDT	7.0 (7.2)	50.6 (52.8)	347 (355)	39.5 (41.5)	0.4 (0.3)	120 (370)
4-min PDT	9.5 (10.0)	58.0 (61.2)	398 (405)	41.1 (42.4)	0.6 (0.4)	1400 (1860)
8-min PDT	9.4 (9.9)	60.8 (64.3)	410 (416)	37.7 (39.1)	0.4 (0.3)	1110 (1340)
12-min PDT	8.8 (9.3)	59.9 (61.7)	395 (403)	37.0 (38.7)	0.5 (0.3)	900 (1230)

the IVT measurements below. The removal of this dominant recombination center improves the recombination losses at the heterointerface. Moreover, the improvement in the optical losses observed in Fig. 3(b) for the 4-min-treated sample adds an additional improvement to the EQE response at longer wavelengths [Fig. 3(a)]. On the other side, the KF PDT adds an additional layer on the surface of the treated absorbers as indicated by the PL measurements below. The effect of this additional layer increases with longer treatment durations leading to increased apparent doping concentrations observed by the CV measurements below and may be responsible for the gradual decrease in the EQE response for the treated samples at longer wavelength regions. Still, a better carrier collection in the bulk of the absorbers with a KF PDT of 4 and 8 min remains. The bandgap determined by linear extrapolation of the long wavelength slope is the same in all samples, unchanged by the PDT. An overall conversion efficiency gain of up to 3% absolute was reached, driven by the higher FF, as well as the improved V_{OC}. The champion cell reaches 10.0% efficiency after both a 4- and 8-min KF PDT. From an IV point of view, an 8-min treatment has slight advantages over the 4-min one in terms of V_{OC}, FF, and R_S while from an optical point of view, the 4-min treatment has a lower reflection and higher J_{SC}. To study the improvement of the V_{OC} in more detail and differentiate between the effects of 4- and 8-min KF PDT, temperature dependent IV measurements have been carried out and the V_{OC} was plotted over the temperature, as depicted in Fig. 4. With a linear fit of the high temperature region (where the solar cell operates) and the extrapolation to 0 K, the activation energy of the main recombination channel is determined [32]. The activation energy for the dominant recombination path at high temperatures of the sample without PDT is well below the bandgap energy, indicating that the sample is dominated by recombination close to the absorber/CdS heterointerface. The corresponding activation energy of the treated samples is much higher (between 950 and 990 meV), very close to the bandgap (995 meV), as determined from the EQE extrapolation, indicating that the main recombination channel is shifted towards the bulk. It should be noted that a complete restoration of the activation energy to the band gap value has been observed with In-Se treatment [9], as well as with *ex situ* KF treatments [14]. The second steeper slope below 150 K of the untreated samples is related to a loss of photocurrent near V_{OC}. Because of this an evaluation with the simple model used is no longer valid. In previous investigation of Cu-rich solar cells similar activation energies (well below the bandgap) were extracted [9,33].

Figure 5 represents the Mott-Schottky plot from the CV measurements at a frequency of 100 kHz for the untreated and the treated cells. The apparent doping is extracted from the slope of the Mott-Schottky plot for each curve in slight forward bias (0.03 – 0.20 V) as indicated by the short dashed lines in Fig. 5. We chose this voltage range because the apparent doping at reverse bias can be influenced by two effects: deep defects would add to the apparent doping [34] or the doping level could be depth dependent [35], due to Cd in-diffusion, reducing the doping level near the interface. In both cases the relevant doping level is extracted at slight forward bias. In simple standard theory the intercept in the Mott-Schottky plot is given by the built-in potential of the junction. In our case, however, the different layers and interfaces can contribute to the capacitance [34,36,37]. We assume that the trends observed for the voltage dependence of the capacitance under slight forward bias do reflect the trends in the space charge region capacitance and can thus be interpreted as

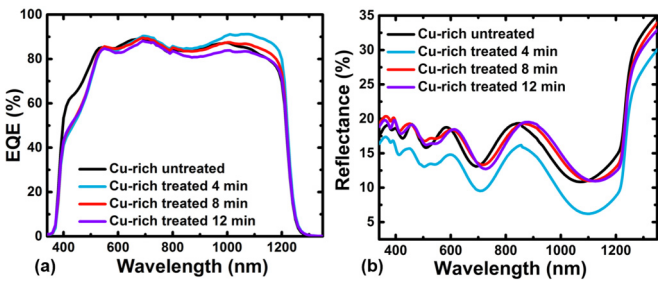

FIG. 3. (a) EQE measurements, (b) Reflection measurements for "Cu-rich" CIS solar cell with and without KF PDT.

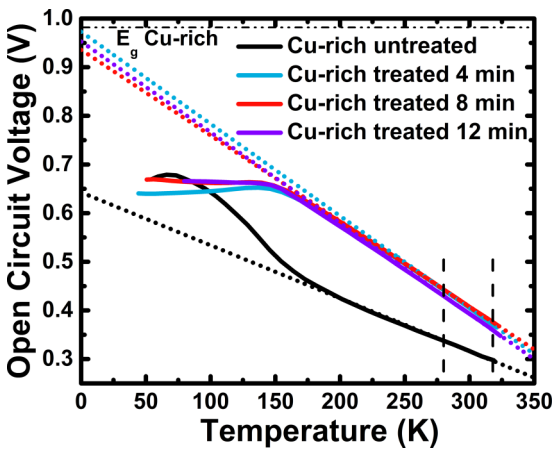

FIG. 4. Temperature dependence of the open circuit voltage for an untreated and treated "Cu-rich" solar cells. A linear fit (dotted line) is used to extract the activation energy. The bandgap (E_G) is represented by a dashed double-dotted line.

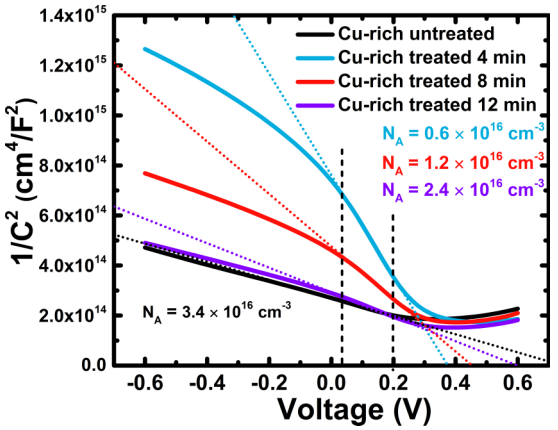

FIG. 5. Capacitance-voltage measurements of an untreated "Cu-rich" solar cell and three cells with different KF deposition times during the PDT. The apparent doping is extracted from the inverse slope of a linear fit at (short dotted lines) small forward bias. The fitting range for all four cells is indicated by the short dashed lines.

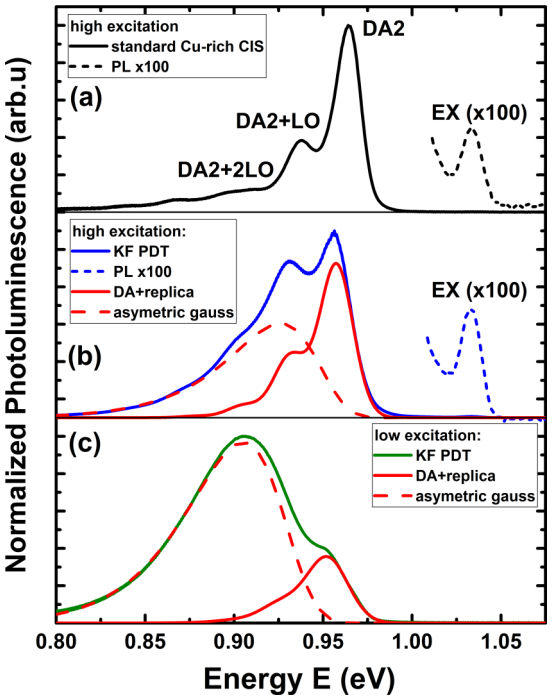

FIG. 6. PL emission spectra measured at 10 K of a "Cu-rich" grown absorber (a) and an absorber with KF PDT measured at high excitation (b) and at low excitation (c). The red lines depict fitting functions used (dashed – asymmetric gauss profile representing a Cu-poor phase, solid – DA transition plus phonon replica representing a "Cu-rich" phase). For better visibility, the peak around 1.03 eV is magnified by a factor of 100.

doping changes. We label this prudently "apparent doping". Based on Fig. 5, it can be observed that the apparent doping decreases after the treatment for all three different treatment durations compared to the untreated cell. This is in accordance with some of the observations in the literature [38], however, an increase has also been observed [26,39]. This decrease in the apparent doping for the three treated samples occurs simultaneously with the removal of a 200 meV defect as presented below. This defect has been reported as an acceptor [31] and removing this defect is responsible for decreasing the apparent doping for all three treated samples. Additionally, it is interesting to observe that the apparent doping increases again as the KF treatment duration increases. The behavior of the apparent doping for the treated samples may be explained by the formation of a Cu-poor layer on the surface of the "Cu-rich" absorber as a result of the KF PDT, as evidenced by the PL measurements below, since the CV measurement investigates mostly the near interface region. This Cu-poor surface layer introduces an additional capacitance and leads to an increase in the apparent doping with longer treatment durations, similar to our Cu-poor cells where the apparent doping of the treated sample is higher than the untreated one. Therefore, this increase in apparent doping with longer treatments indicates that the apparent doping may not be the actual doping in the absorber but is related to the additional layer and hence, the interpretation in terms of a simple one-sided abrupt junction may not be applicable in this context [40]. In summary, the treatment removes the 200 meV defect and forms a Cu-poor surface. This Cu-poor surface behaves very similar to a Cu-poor absorber with longer treatment time.

What happens in detail at the surface with a KF PDT is still under debate. Studies on Cu-poor cells suggest that the surface is completely depleted of Cu after KF PDT forming a new compound consisting of potassium, indium, and selenium (KIS) improving the heterojunction [25,29]. After an *ex situ* treatment of a "Cu-rich" sample, reduced but considerable amounts of Cu have been detected at the surface, and with changed chemical bonds [14]. A tool to distinguish between "Cu-rich" and Cu-poor material is low temperature PL, as long as the phases are present in sufficient quantity [41]. PL measurements at 10 K under various illumination intensities are carried out on the untreated and treated absorber layers. All samples are bare absorbers; not covered with CdS or any further layers. Since the results of the samples with PDT are similar, only the sample with 8-min KF PDT is compared to the reference. Figure 6 displays the normalized PL spectra of an untreated sample (a) and the KF treated sample at high excitation (b) and at low excitation (c). The untreated sample shows the well-known peaks of "Cu-rich" $CuInSe_2$ [41]. Cu-rich and Cu-poor CIS have very distinctive "fingerprints" in their PL spectra [24,41,42]. Cu-rich material shows narrow peaks and excitonic luminescence, whereas Cu-poor material shows one broad peak, red shifting with increasing Cu deficit. The broadening and the redshift are due to potential fluctuations. The spectrum of the untreated sample [Fig. 6(a)] is a clear "Cu-rich" spectrum. The peak at 0.97 eV is a donor-acceptor pair transition commonly denoted as DA2. The two peaks at 0.94 and 0.91 eV are phonon replica (+LO) of the DA2 transition. The corresponding LO phonon has an energy of 26 meV. At 1.03 eV a weak but distinct peak originating from excitonic transitions is measured. The PL spectrum of the treated sample at low excitation [Fig. 6(c)] shows the typical asymmetric and redshifted peak of Cu-poor CIS, plus a shoulder at higher energies. The origin of this shoulder can be understood by investigating the spectrum at higher intensities [Fig. 6(b)], where excitonic luminescence becomes visible and the former shoulder becomes the main peak, accompanied

by a phonon replica. The broad luminescence is still visible, but blue shifted compared to the peak at low intensities which is expected for the luminescence of Cu-poor CIS. This is a spectrum one would expect from a combination of the luminescence from Cu-rich and from Cu-poor CIS. This can be further corroborated from intensity dependent measurements where both spectra behave differently. With increasing excitation, the left peak shifts with 14 meV/decade, typical for the broad luminescence of Cu-poor material with potential fluctuations, whereas the right one shifts with less than 5 meV/decade, typical for DA transitions. The exponent of the power law between the PL intensity and the excitation intensity is higher for the right peak, describing a faster increase with excitation. Both properties indicate that the two peaks originate from different transitions. All spectra can be fitted with the known spectra from a "Cu-rich" absorber with the DA2 transition (plus phonon replica) [43] plus an asymmetric Gauss peak, representing the PL from a Cu-poor phase. The fit matches the spectra over the three orders of magnitude of excitation measured. The fact that DA2 transition in the treated sample is a little redshifted from the untreated one is not worrisome. The fitted spectrum with the exciton is absolutely typical for Cu-rich CIS and the shift could have various reasons, like incomplete background correction from the broad peak or the lower excitation density in the bulk of the treated sample, since the excitation is partly absorbed in the Cu-poor phase. From the fitting of the PL spectra, it can be deduced that within the probed surface region of a few hundred nanometers, a Cu-poor as well as a "Cu-rich" phase exist. Formerly it was assumed that the addition of KF during the PDT pushes the copper atoms from the surface into the bulk leading to a new copper deficient layer. According to the phase diagram no Cu-rich CIS phase exists [11], the bulk is saturated with Cu, and the in-diffusion of Cu is not possible for stoichiometric CIS samples as used here. Thus, it can be concluded that the new phase grows during the KF PDT on top of the absorber layer, combining the potassium and Se atoms from the gas phase with Cu and In atoms from the absorber. This assumption of the growth is supported by the fact that, for the longest treatment duration also the DA1 transition is observed in low temperature PL measurements. The DA1 transition has the same donor as the DA2 transition, but the acceptor is shallower and commonly attributed to the copper vacancy. This means that during the KF PDT copper atoms diffused from the bulk into the new layer. Taking the penetration depth of the laser excitation as well as the relative photoluminescence yield of both phases into account, the newly grown copper deficient layer is estimated to be thinner than 20 nanometer. This estimated maximal thickness agrees with values reported in literature of a few nanometers [26] on copper deficient samples as well as with values reported for samples grown under Cu-excess [14].

In addition to the above improvements provided by the KF PDT to the surface of the "Cu-rich" absorbers, the temperature and frequency dependent capacitance measurements revealed an additional change in the electronic structure of "Cu-rich" based solar cells. We measure the temperature and frequency dependence of the capacitance of the solar cells, which allows conclusions on defects and barriers [34]. In general, the admittance measurements of untreated "Cu-rich" $CuInSe_2$ is characterized by one dominant capacitance step

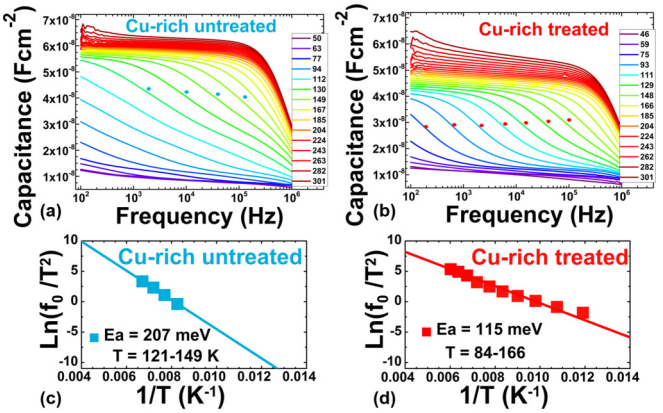

FIG. 7. Admittance measurements for "Cu-rich" CIS solar cells (a) without KF PDT and (b) with a 4-min KF PDT for temperatures between 50 and 300 K. The Arrhenius plot indicates the activation energy of the main capacitance step for absorbers (c) without treatment and (d) with 4-min treatment.

with an activation energy around 200 meV, as presented in Figs. 7(a) and 7(c) [44]. This step shows a second signature at higher frequencies/lower temperatures, which cannot be analyzed in detail, since the inflection points are not observed. This dominant step in "Cu-rich" solar cells can be removed by the In-Se treatment [45]. The KF treatment presented in this contribution also removes this main step, as observed in Figs. 7(b) and 7(d). The main step observed after the treatment has a lower activation energy of around 100–150 meV. It is likely that this step is the hidden second signature seen in the sample without treatment. The origin of this 200-meV step could be either a defect or a barrier that is removed by the treatment [31]. We note that all treatments we have tested on "Cu-rich" absorbers: In-Se treatment [9], *ex situ* KF treatment [14], or the KF treatment with etching step discussed here, remove this admittance signature.

To check at which stage in the solar cell preparation the improvement by the KF treatment becomes manifest, we measure qFLs of treated and untreated absorbers. Absolute calibrated measurements are carried out on untreated absorber layers which have been KCN etched and covered with CdS as well as on treated absorber layers covered with CdS. The deposition of CdS is necessary to prevent the oxidation of the absorber surface and thus the degradation of the qFLs [7,18]. A second sample set was investigated to correlate solar cell improvements and qFLs. This second set shows similar improvements of the efficiency and increase in V_{OC} (343 mV to 393 mV) compared to the sample set presented so far. The gain of 50 meV in V_{OC} is a bit lower but comparable to the first set (60 mV). A qFLs of 467 meV is determined for the sample without treatment and a qFLs of 486 meV after the KF PDT under the equivalent illumination of 1 sun, leading to an improvement of about 20 meV. The same trend, that the gain in V_{OC} is about twice as high as in the qFLs, has been observed in all Cu-rich samples that we investigated, independent of the exact treatment conditions. This shows that the non-radiative recombination is reduced even before the junction formation by the TCO deposition. The additional gain in V_{OC} compared to the gain in qFLs indicates that both bulk and interface

are improved. For Cu-poor CIS samples with KF PDT the gain in qFLs of about 20 meV (451–470 meV) is roughly the same, showing that the absorber improvement works similar in both material compositions. But the gain of V_{OC} of 22 mV (445–467 mV) is within error the same as the gain in qFLs, showing that only the bulk is improved. Recent measurements on Cu-poor CIGS show a similar effect [46].

B. KF PDT with etching step on Cu-poor absorber layers

To check if the effectiveness of the KF PDT route presented in this contribution is specific to "Cu-rich" absorbers, Cu-poor absorbers are treated in the same way including a short KCN etch after absorber deposition. The power conversion efficiency for this specific absorber improves on average from 11.8 to 13.0%. The improvement is driven by an increase in the V_{OC} (445–467 mV) with an additional increase in FF (64.0–68.3%), as can be seen in Fig. 8(a). J_{SC} decreases slightly (41.3−40.8 mA/cm^2). This is linked to a lower spectral response in the short wavelength region due to a thicker CdS layer, Fig. 8(b). The thickness of the CdS layer without treatment is (34 ± 3) nm comparable to the "Cu-rich" grown absorber. The increase of the CdS thickness, as determined from SEM cross sections, after KF PDT [(43 ± 2) nm] is less pronounced in the Cu-poor sample, corresponding to the less pronounced drop in QE. The shunt resistances and series resistances are unchanged within error. In both samples, the activation energy of the main recombination channel extrapolates near the bandgap in IV(T) measurements showing that the samples are dominated by bulk recombination, Fig. 8(c). CV measurements show that the apparent doping stayed unchanged within error before and after the KF PDT (1.3×10^{16} cm^{-3} to 1.5×10^{16} cm^{-3}), Fig. 8(d). It is important to note that most of our treated Cu-poor CIS cells experienced an increase in the apparent doping after the KF PDT as it has been reported before in literature [26,39]. Finally, it can be deduced that the KF PDT with etching step improves both "Cu-rich" and Cu-poor CIS samples and is a beneficial postdeposition process.

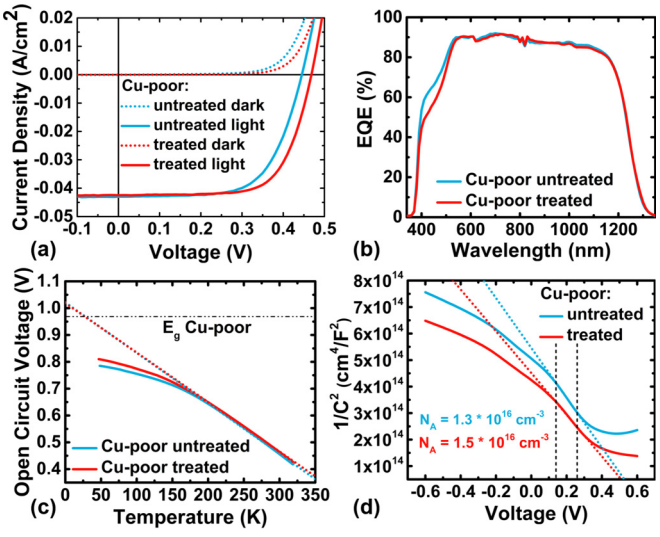

FIG. 8. Electrical characterization of a Cu-poor CIS sample before and after a 6-min KF PDT in terms of (a) IV, (b) EQE, and (c) IV(T). The short dotted lines indicate the extrapolated activation energy to zero Kelvin. The dashed double-dotted line indicates the bandgap of Cu-poor cells. (d) CV measurements. The short dotted lines indicate the fit from where the apparent doping is extracted. The short dashed lines (black) indicate the region of fitting.

IV. CONCLUSION

We use the fundamental differences in the dominating recombination path between Cu-rich and Cu-poor $CuInSe_2$ to study the effects of the alkali postdeposition treatment. It is well known that Cu-rich $CuInSe_2$ solar cells are dominated by interface recombination [6], whereas the standard Cu-poor material is controlled by bulk recombination. We develop a potassium postdeposition treatment that can be applied to Cu-rich material, where an additional etching step is necessary. The same postdeposition treatment with etching step is applied to Cu-poor material. In both cases we observe an increase in the power conversion efficiency, mostly due to improvements of the V_{OC} and the FF. The improvements are stronger in the Cu-rich case. It has been shown before that the treatment creates a completely or partly Cu depleted surface in Cu-poor absorbers [3,25,29]. Here we show by low temperature PL that also on the surface of Cu-rich $CuInSe_2$ a Cu-poor layer is formed. Since the bulk of $CuInSe_2$ grown under Cu-excess is saturated with copper, the Cu-poor surface cannot be formed by in-diffusion of Cu but has to be grown during the treatment by out-diffusion of Cu. Calibrated photoluminescence measurements are used to determine how the treatment impacts the qFLs. In both cases, Cu-rich and Cu-poor, a comparable increase of about 20 meV is observed. In Cu-poor solar cells this corresponds approximately to the increase in open circuit voltage, indicating that the positive effect is mostly due to changes in the bulk of the absorber. The improvement in the V_{OC} of Cu-rich solar cells, however, is about twice as high as the improvement in the qFLs, indicating that an additional improvement beyond the bulk is active. This is due to an improved interface. The dominating recombination path shifts from the interface to the bulk in Cu-rich solar cells, as indicated by the temperature dependent extrapolation of the open circuit voltage. This could be related to the removal of 200 meV deep defect, as observed from admittance spectroscopy. In summary the KF postdeposition treatment improves the bulk recombination and forms a Cu depleted surface independent of the composition. The first is observed in an improved quasi-Fermi level splitting and thus higher V_{OC}, both in Cu-rich and Cu-poor. However, the formation of a Cu-poor surface is only important if the cell is dominated by recombination close to the interface before the treatment.

ACKNOWLEDGMENT

This contribution has been funded by the Luxembourgish Fonds National de la Recherche (FNR) in the framework of the CURI-K project, which is gratefully acknowledged.

[1] P. Jackson, R. Wuerz, D. Hariskos, E. Lotter, W. Witte, and M. Powalla, Effects of heavy alkali elements in Cu(In, Ga)Se_2 solar cells with efficiencies up to 22.6%, Phys. Status Solidi - Rapid Res. Lett. **10**, 583 (2016).

[2] Solar Frontier Achieves World Record Thin-Film Solar Cell Efficiency of 22.9% (2017) [Online]. Available at http://www.solar-frontier.com/eng/news/2017/1220_press.html

[3] A. Chirilă, P. Reinhard, F. Pianezzi, P. Bloesch, A. R. Uhl, C. Fella, L. Kranz, D. Keller, C. Gretener, H. Hagendorfer, D. Jaeger, R. Erni, S. Nishiwaki, S. Buecheler, and A. N. Tiwari, Potassium-induced surface modification of Cu(In, Ga)Se_2 thin films for high-efficiency solar cells, Nat. Mater. **12**, 1107 (2013).

[4] J. AbuShama, R. Noufi, S. Johnston, S. Ward, and X. Wu, Improved performance in $CuInSe_2$ and surface-modified $CuGaSe_2$ solar cells, in *Conference Record of the Thirty-first IEEE Photovoltaic Specialists Conference* (IEEE, 2005), pp. 299–302.

[5] S. Siebentritt, L. Gütay, D. Regesch, Y. Aida, and V. Deprédurand, Why do we make Cu(In, Ga)Se_2 solar cells non-stoichiometric? Sol. Energy Mater. Sol. Cells **119**, 18 (2013).

[6] M. Turcu, O. Pakma, and U. Rau, Interdependence of absorber composition and recombination mechanism in Cu(In,Ga)$(Se,S)_2$ heterojunction solar cells, Appl. Phys. Lett. **80**, 2598 (2002).

[7] F. Babbe, L. Choubrac, and S. Siebentritt, Quasi Fermi level splitting of Cu-rich and Cu-poor Cu(In,Ga)Se_2 absorber layers, Appl. Phys. Lett. **109**, 082105 (2016).

[8] T. Bertram, V. Deprédurand, and S. Siebentritt, In-Se surface treatment of Cu-rich grown $CuInSe_2$, in *2014 IEEE 40th Photovoltaic Specialist Conference (PVSC)* (IEEE, 2014), pp. 3633–3636.

[9] Y. Aida, V. Deprédurand, J. K. Larsen, H. Arai, D. Tanaka, M. Kurihara, and S. Siebentritt, Cu-rich $CuInSe_2$ solar cells with a Cu-poor surface, Prog. Photovoltaics Res. Appl. **23**, 754 (2015).

[10] L. Choubrac, T. Bertram, H. Elanzeery, and S. Siebentritt, Cu(In,Ga)Se_2 solar cells with improved current based on surface treated stoichiometric absorbers, Phys. Status Solidi **214**, 1600482 (2017).

[11] T. Gödecke, T. Haalboom, and F. Ernst, Phase equilibria of Cu-In-Se I. The In_2Se_3-Se-Cu_2Se subsystem, Z. Metallkd. **91**, 622 (1948).

[12] Y. Hashimoto, N. Kohara, T. Negami, M. Nishitani, and T. Wada, Surface characterization of chemically treated Cu(In,Ga)Se_2 thin films, Jpn. J. Appl. Phys. **35**, 4760 (1996).

[13] V. Deprédurand, D. Tanaka, Y. Aida, M. Carlberg, N. Fèvre, and S. Siebentritt, Current loss due to recombination in Cu-rich $CuInSe_2$ solar cells, J. Appl. Phys. **115**, 044503 (2014).

[14] H. Elanzeery, F. Babbe, M. Melchiorre, A. Zelenina, and S. Siebentritt, Potassium fluoride ex situ treatment on both Cu-rich and Cu-poor $CuInSe_2$ thin film solar cells, IEEE J. Photovoltaics **7**, 684 (2017).

[15] P. Pistor, D. Greiner, C. A. Kaufmann, S. Brunken, M. Gorgoi, A. Steigert, W. Calvet, I. Lauermann, R. Klenk, T. Unold, and M. C. Lux-Steiner, Experimental indication for band gap widening of chalcopyrite solar cell absorbers after potassium fluoride treatment, Appl. Phys. Lett. **105**, 063901 (2014).

[16] V. Deprédurand, T. Bertram, and S. Siebentritt, Influence of the Se environment on Cu-rich CIS devices, Phys. B Condens. Matter **439**, 101 (2014).

[17] See Supplemental Material at http://link.aps.org/supplemental/10.1103/PhysRevMaterials.2.105405 for SEM images and EDX data before and after KCN etching, top view and cross-section SEM images of treated and untreated absorber layers.

[18] D. Regesch, L. Gütay, J. K. Larsen, V. Deprédurand, D. Tanaka, Y. Aida, and S. Siebentritt, Degradation and passivation of $CuInSe_2$, Appl. Phys. Lett. **101**, 112108 (2012).

[19] B. Canava, J.-F. Guillemoles, J. Vigneron, D. Lincot, and A. Etcheberry, Chemical elaboration of well defined Cu(In, Ga)Se_2 surfaces after aqueous oxidation etching, J. Phys. Chem. Solids **64**, 1791 (2003).

[20] V. Deprédurand, T. Bertram, D. Regesch, B. Henx, and S. Siebentritt, The influence of Se pressure on the electronic properties of $CuInSe_2$ grown under Cu-excess, Appl. Phys. Lett. **105**, 172104 (2014).

[21] M. Hála, H. Kato, M. Algasinger, Y. Inoue, G. Rey, F. Werner, C. Schubbert, T. Dalibor, and S. Siebentritt, Improved environmental stability of highly conductive nominally undoped ZnO layers suitable for n-type windows in thin film solar cells, Sol. Energy Mater. Sol. Cells **161**, 232 (2017).

[22] M. Hála, S. Fujii, A. Redinger, Y. Inoue, G. Rey, M. Thevenin, V. Deprédurand, T. P. Weiss, T. Bertram, and S. Siebentritt, Highly conductive ZnO films with high near infrared transparency, Prog. Photovoltaics Res. Appl. **23**, 1630 (2015).

[23] P. Wurfel, The chemical potential of radiation, J. Phys. C Solid State Phys. **15**, 3967 (1982).

[24] T. Unold and L. Gütay, Photoluminescence analysis of thin-film solar cells, in *Advanced Characterization Techniques for Thin Film Solar Cells*, edited by D. Abou-Ras, T. Kirchartz, and U. Rau (Wiley-VCH Verlag GmbH & Co. KGaA, Weinheim, Germany, 2011), Vol. 1–2, pp. 151–175.

[25] P. Reinhard, B. Bissig, F. Pianezzi, H. Hagendorfer, G. Sozzi, R. Menozzi, C. Gretener, S. Nishiwaki, S. Buecheler, and A. N. Tiwari, Alkali-templated surface nanopatterning of chalcogenide thin films: A novel approach toward solar cells with enhanced efficiency, Nano Lett. **15**, 3334 (2015).

[26] I. Khatri, H. Fukai, H. Yamaguchi, M. Sugiyama, and T. Nakada, Effect of potassium fluoride post-deposition treatment on Cu(In,Ga)Se_2 thin films and solar cells fabricated onto sodalime glass substrates, Sol. Energy Mater. Sol. Cells **155**, 280 (2016).

[27] A. Zelenina, F. Werner, H. Elanzeery, M. Melchiorre, and S. Siebentritt, Space-charge-limited currents in CIS-based solar cells, Appl. Phys. Lett. **111**, 213903 (2017).

[28] A. R. Burgers, J. A. Eikelboom, A. Schonecker, and W. C. Sinke, Improved treatment of the strongly varying slope in fitting solar cell I-V curves, in *Conference Record of the Twenty Fifth IEEE Photovoltaic Specialists Conference* (IEEE, 1996), pp. 569–572.

[29] P. Reinhard, B. Bissig, F. Pianezzi, E. Avancini, H. Hagendorfer, D. Keller, P. Fuchs, M. Döbeli, C. Vigo, P. Crivelli, S. Nishiwaki, S. Buecheler, and A. N. Tiwari, Features of KF and NaF postdeposition treatments of Cu(In,Ga)Se_2 absorbers for high efficiency thin film solar cells, Chem. Mater. **27**, 5755 (2015).

[30] A. Nakane, H. Tampo, M. Tamakoshi, S. Fujimoto, K. M. Kim, S. Kim, H. Shibata, S. Niki, and H. Fujiwara, Quantitative determination of optical and recombination losses in thin-film photovoltaic devices based on external quantum efficiency analysis, J. Appl. Phys. **120**, 064505 (2016).

[31] H. Elanzeery, M. Melchiorre, F. Babbe, M. Sood, F. Werner, and S. Siebentritt, Surface treatments unveil defects in Cu-rich CIS thin film solar cells (unpublished).

[32] S. S. Hegedus and W. N. Shafarman, Thin-film solar cells: device measurements and analysis, Prog. Photovoltaics Res. Appl. **12**, 155 (2004).

[33] V. Deprédurand, Y. Aida, J. K. Larsen, T. Eisenbarth, A. Majerus, and S. Siebentritt, Surface treatment of CIS solar cells grown under Cu-excess, in *2011 37th IEEE Photovoltaic Specialists Conference* (IEEE, 2011), pp. 000337–000342.

[34] J. Heath and P. Zabierowski, Capacitance spectroscopy of thin-film solar cells, in *Advanced Characterization Techniques for Thin Film Solar Cells* (Wiley-VCH Verlag GmbH & Co. KGaA, Weinheim, Germany, 2011), pp. 81–105.

[35] F. Werner, T. Bertram, J. Mengozzi, and S. Siebentritt, What is the dopant concentration in polycrystalline thin-film Cu(In, Ga)Se_2? Thin Solid Films **633**, 222 (2017).

[36] T. Eisenbarth, T. Unold, R. Caballero, C. A. Kaufmann, and H.-W. Schock, Interpretation of admittance, capacitance-voltage, and current-voltage signatures in Cu(In, Ga)Se_2 thin film solar cells, J. Appl. Phys. **107**, 034509 (2010).

[37] G. Sozzi, M. Lazzarini, R. Menozzi, R. Carron, E. Avancini, B. Bissig, S. Buecheler, and A. N. Tiwari, A numerical study of the use of C-V characteristics to extract the doping density of CIGS absorbers, in *2016 IEEE 43rd Photovoltaic Specialists Conference (PVSC)* (IEEE, 2016), pp. 2283–2288.

[38] F. Pianezzi, P. Reinhard, A. Chirilă, B. Bissig, S. Nishiwaki, S. Buecheler, and A. N. Tiwari, Unveiling the effects of post-deposition treatment with different alkaline elements on the electronic properties of CIGS thin film solar cells, Phys. Chem. Chem. Phys. **16**, 8843 (2014).

[39] A. Laemmle, R. Wuerz, and M. Powalla, Efficiency enhancement of Cu(In, Ga)Se_2 thin-film solar cells by a post-deposition treatment with potassium fluoride, Phys. Status Solidi - Rapid Res. Lett. **7**, 631 (2013).

[40] F. Werner, A. Zelenina, and S. Siebentritt, Experimental evidence for CdS-related transport barrier in thin film solar cells and its impact on admittance spectroscopy, in *Proceedings of IEEE Photovoltaics Specialist Conference (PVSC)* (IEEE, 2017).

[41] S. Siebentritt, N. Rega, A. Zajogin, and M. C. Lux-Steiner, Do we really need another PL study of $CuInSe_2$? Phys. Status Solidi **1**, 2304 (2004).

[42] I. Dirnstorfer, M. Wagner, D. M. Hofmann, M. D. Lampert, F. Karg, and B. K. Meyer, Characterization of CuIn(Ga)Se_2 thin films, Phys. Status Solidi **168**, 163 (1998).

[43] A. Alkauskas, M. D. McCluskey, and C. G. Van de Walle, Tutorial: Defects in semiconductors—Combining experiment and theory, J. Appl. Phys. **119**, 181101 (2016).

[44] T. Bertram, V. Depredurand, and S. Siebentritt, Electrical characterization of defects in Cu-rich grown $CuInSe_2$ solar cells, IEEE J. Photovoltaics **6**, 546 (2016).

[45] T. Bertram, Doping, Defects And Solar Cell Performance Of Cu-rich Grown $CuInSe_2$ (2016). [Online]. Available at http://orbilu.uni.lu/handle/10993/28325

[46] M. H. Wolter, B. Bissig, E. Avancini, R. Carron, S. Buecheler, P. Jackson, and S. Siebentritt, Influence of sodium and rubidium postdeposition treatment on the quasi-Fermi level splitting of Cu(In, Ga)Se_2 thin films, IEEE J. Photovoltaics **8**, 1320 (2018).